Supplementary Information (SI) for Materials Advances.
This journal is © The Royal Society of Chemistry 2025

Optical studies of stimuli-responsive organic crystals differing in the position and nature of functional groups

Sumeera Farooq,[a] Ishtiyaq Ahmad,[a] and Aijaz A. Dar *[a]

Keywords: Crystal engineering, functional thin films, structure-property corelation, thermochromism, mechanochromism

Corresponding authors: aijazku2015@gmail.com/daraijaz@uok.edu.in,Orcid: 0000-0002-6180-274X

Electronic Supporting information

Figure S-34: Thermochromic photoghaphs under different conditions in **3H**.
Table S-1: Crystallographic Table of **1-3**
Table S-2: The calculated energy levels for **1-3**
Table S-3: LODs values of some selective zinc sensors.
Table S-4: Interaction and lattice energy calculation of **1.**
Table S-5: Interaction and lattice energy calculation of **2.**
Table S-6: Interaction and lattice energy calculation of **3.**

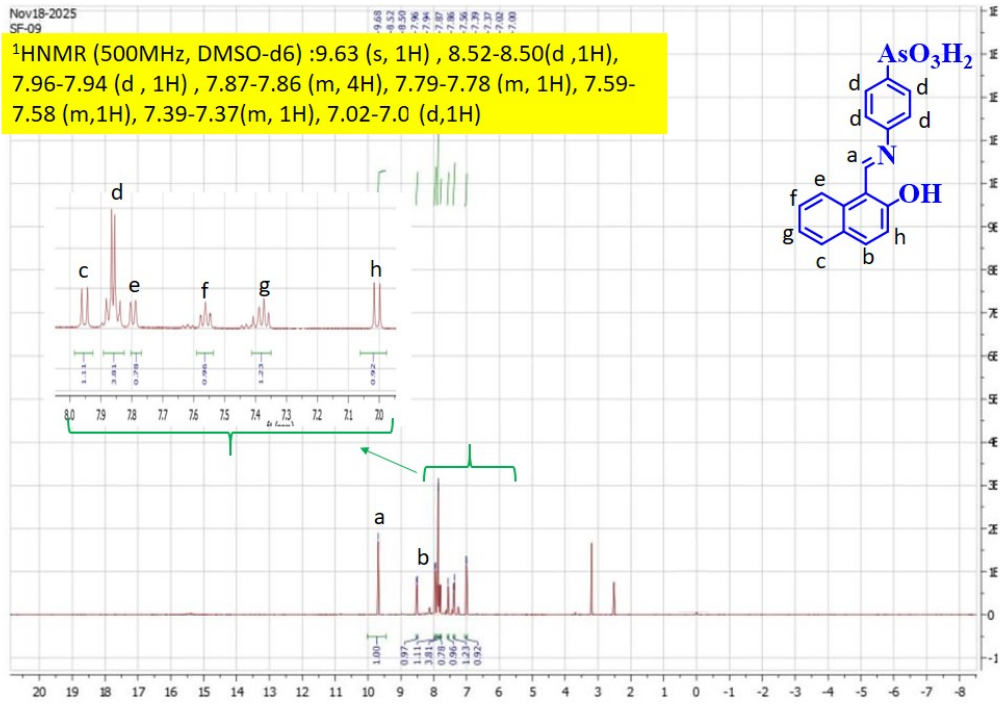

Figure S-1:[1]H NMR spectra of **1** recorded in DMSO-d_6 solvent (500MHz).

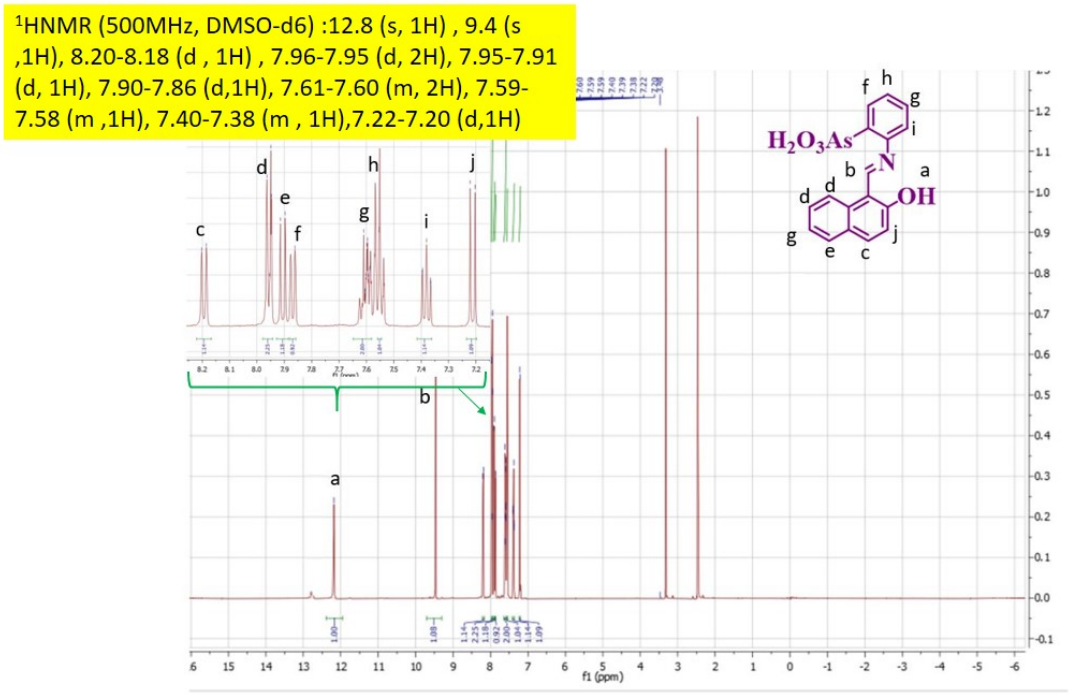

Figure S-2: ^{1}H NMR spectra of **2** recorded in DMSO-d_6 solvent (500MHz).

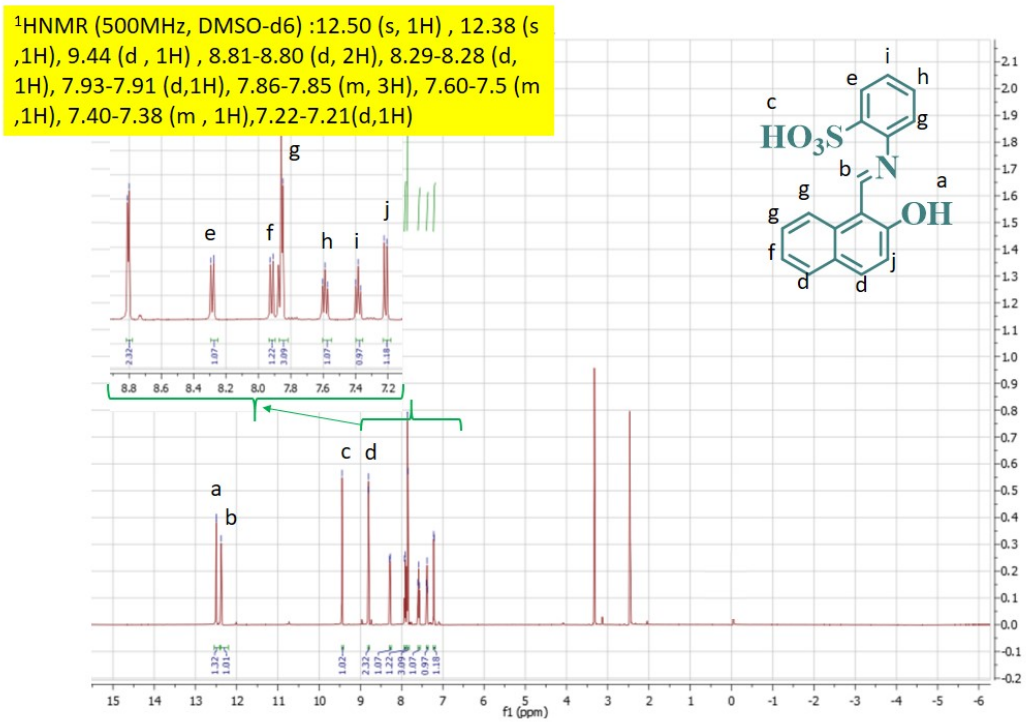

Figure S-3: ^{1}H NMR spectra of **3** recorded in DMSO-d_6 solvent (500MHz).

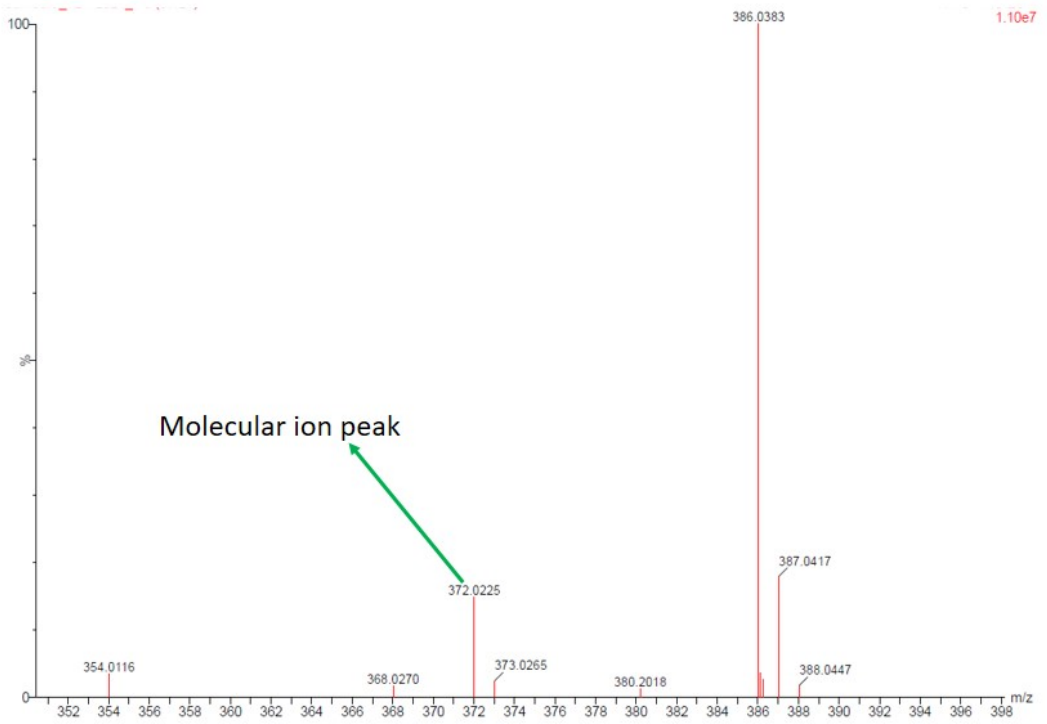

Figure S-4: HR-MS spectra of **1**

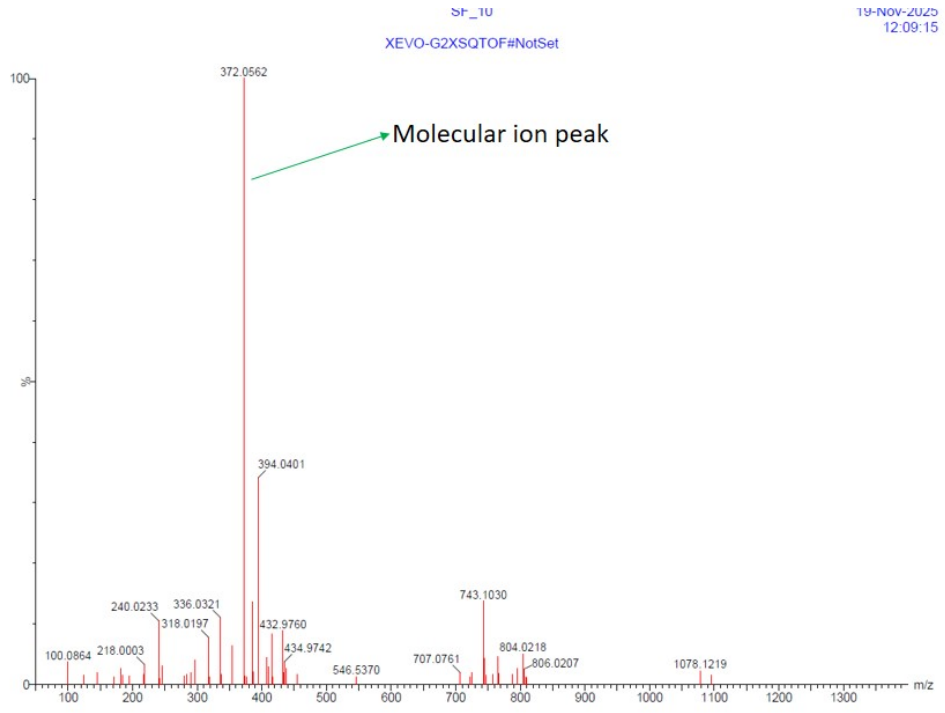

Figure S-5: HR-MS spectra of **2**

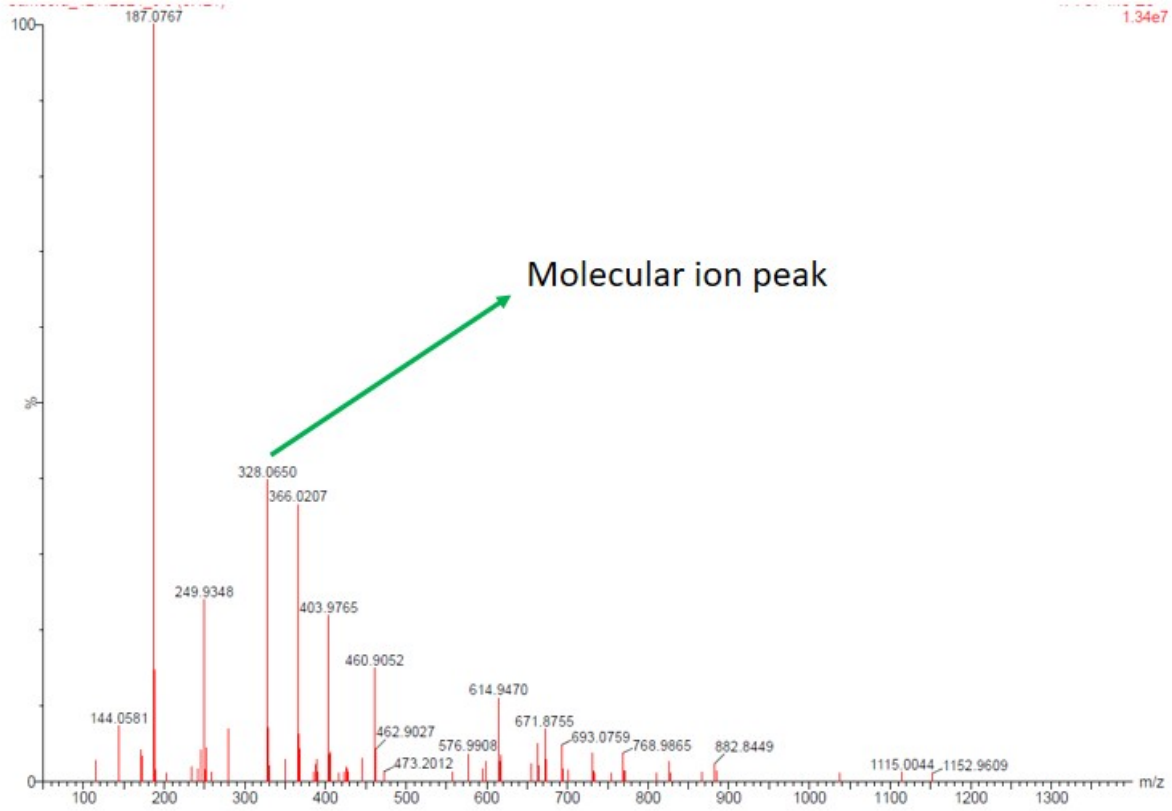

Figure S-6: HR-MS spectra of **3**

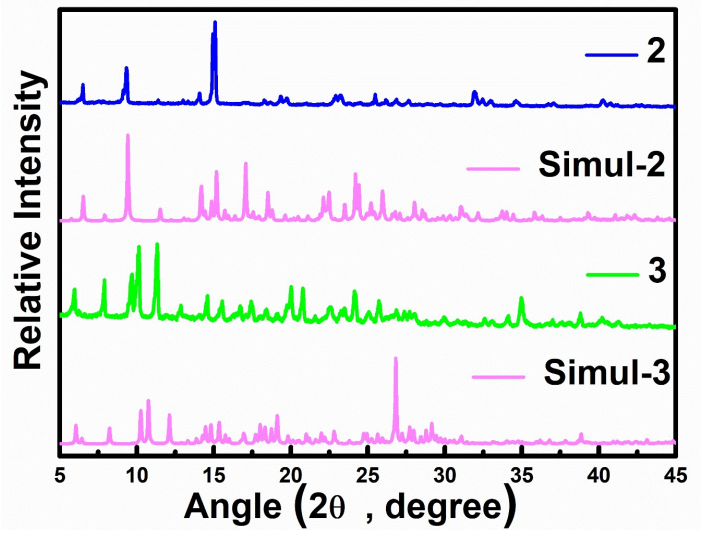

Figure S-7: PXRD spectra of **2** and **3.**

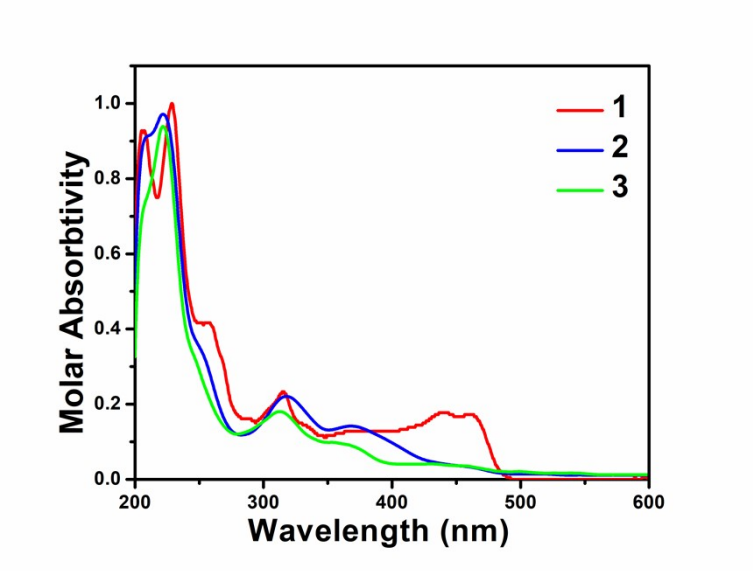

Figure S-8-: Solution phase Absorption spectra of **1-3** in MeOH (10^{-5}M conc.).

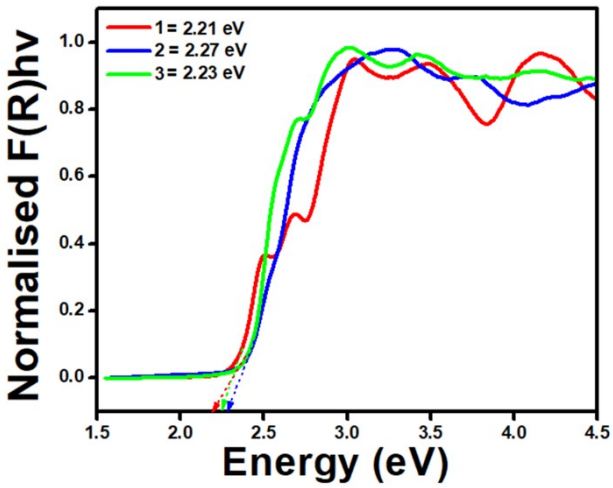

Figure S-9: Tauc plots of **1-3** depicting the band gaps.

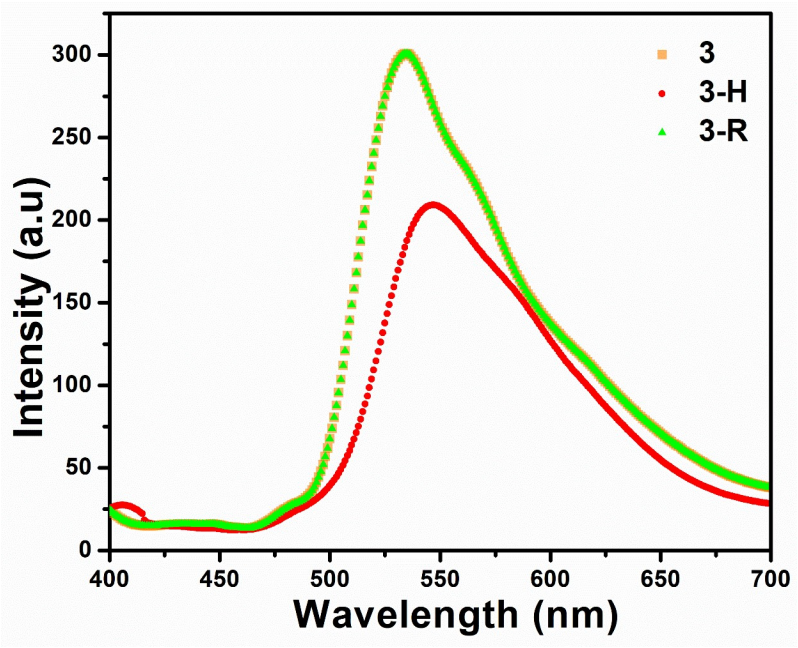

Figure S-10: Luminescence spectra of **3** displaying changes in luminescence upon heating.

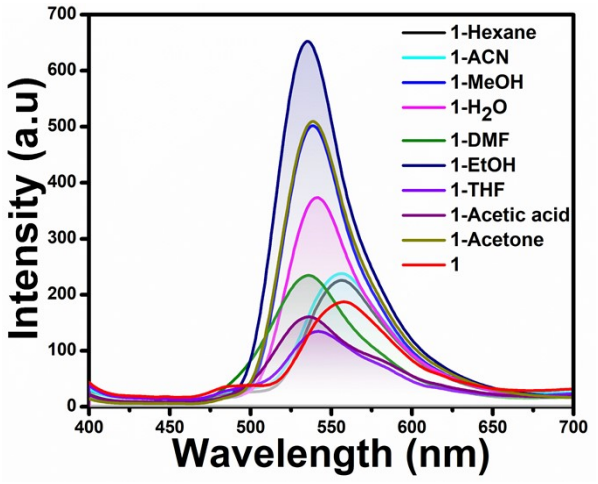

Figure S-11: Emission spectra of thin films of **1.**

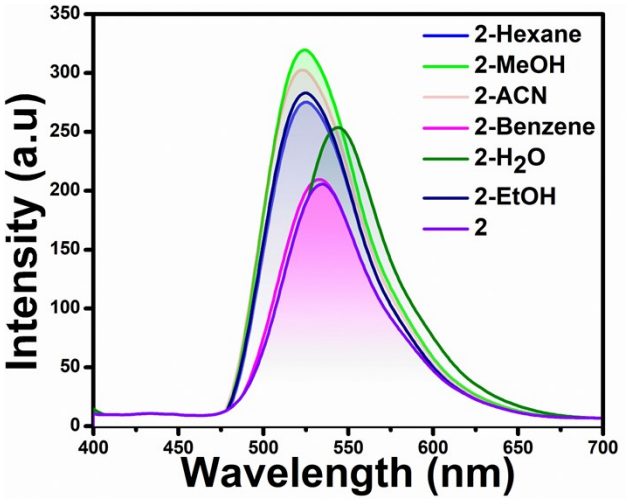

Figure S-12: Emission spectra of thin films of **2.**

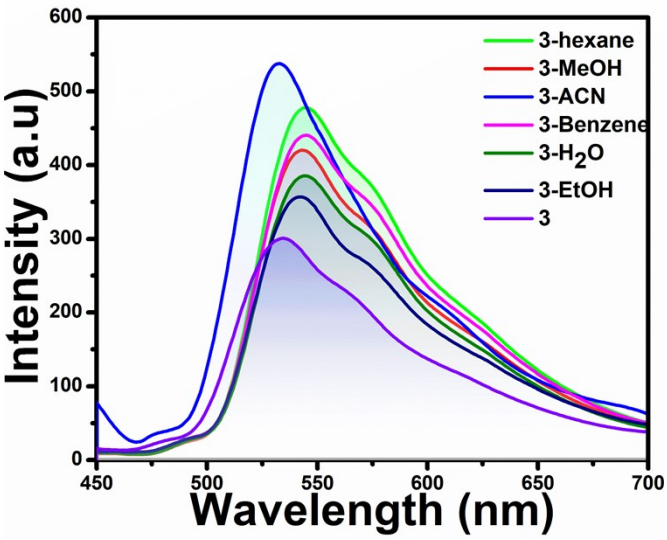

Figure S-13: Emission spectra of thin films of **3**

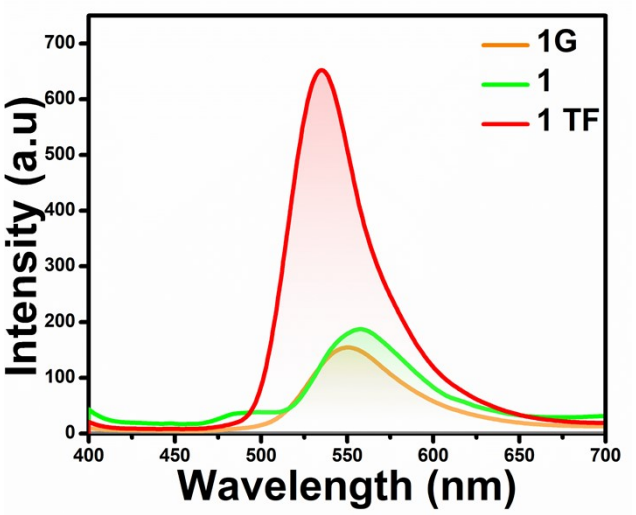

Figure S-14: Emission spectra of crystal, powder and thin film of **1.**

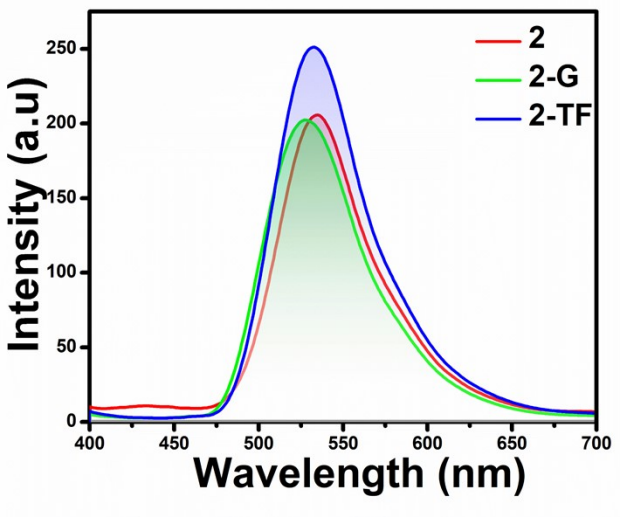

Figure S-15: Emission spectra of crystal, powder and thin film of **2.**

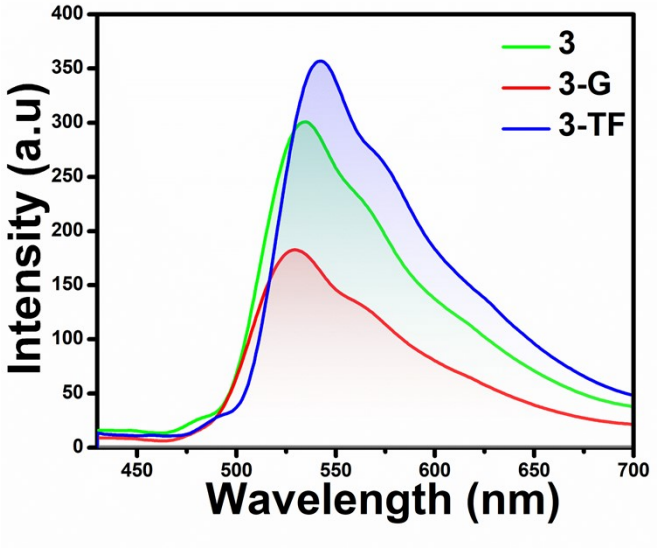

Figure S-16: Emission spectra of crystal, powder and thin film of **3.**

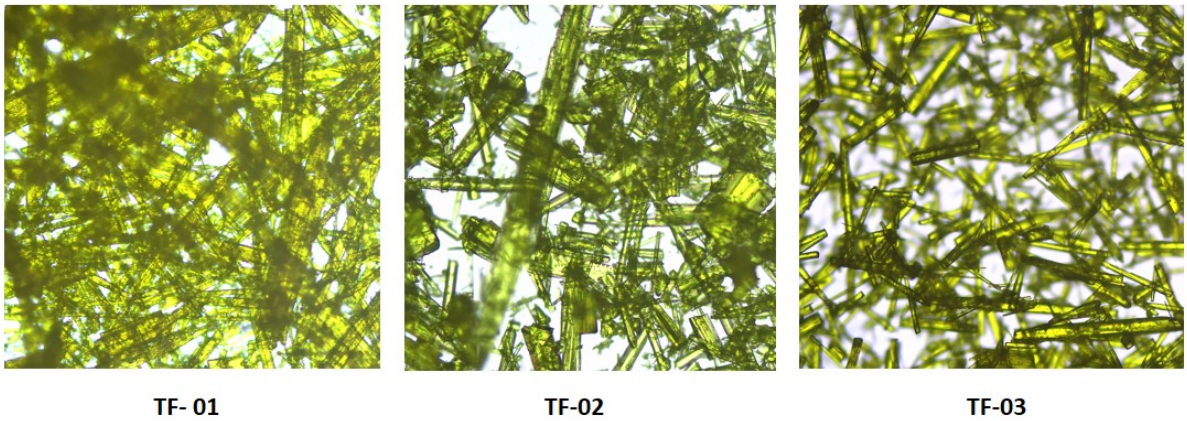

Figure S-17: Crystal morphologies of thin films **1- 3.**

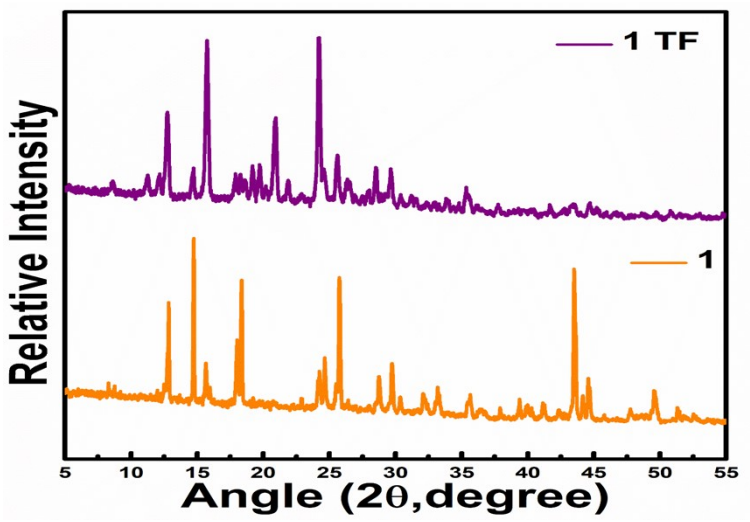

Figure S-18: Pxrd of thin film in EtOH of **1.**

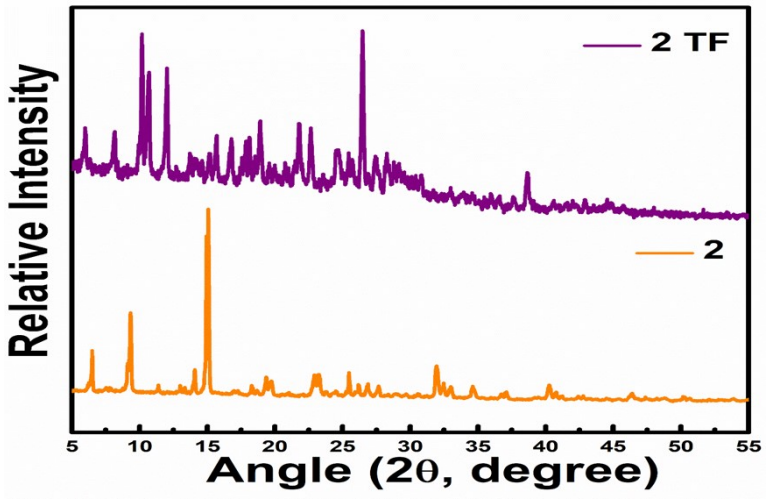

Figure S-19: Pxrd of thin film in EtOH of **2.**

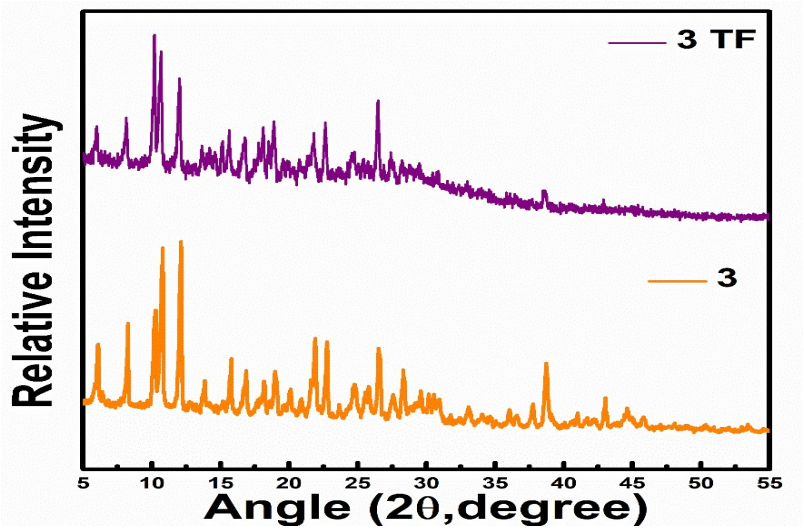

Figure S-20: Pxrd of thin film in EtOH of **3.**

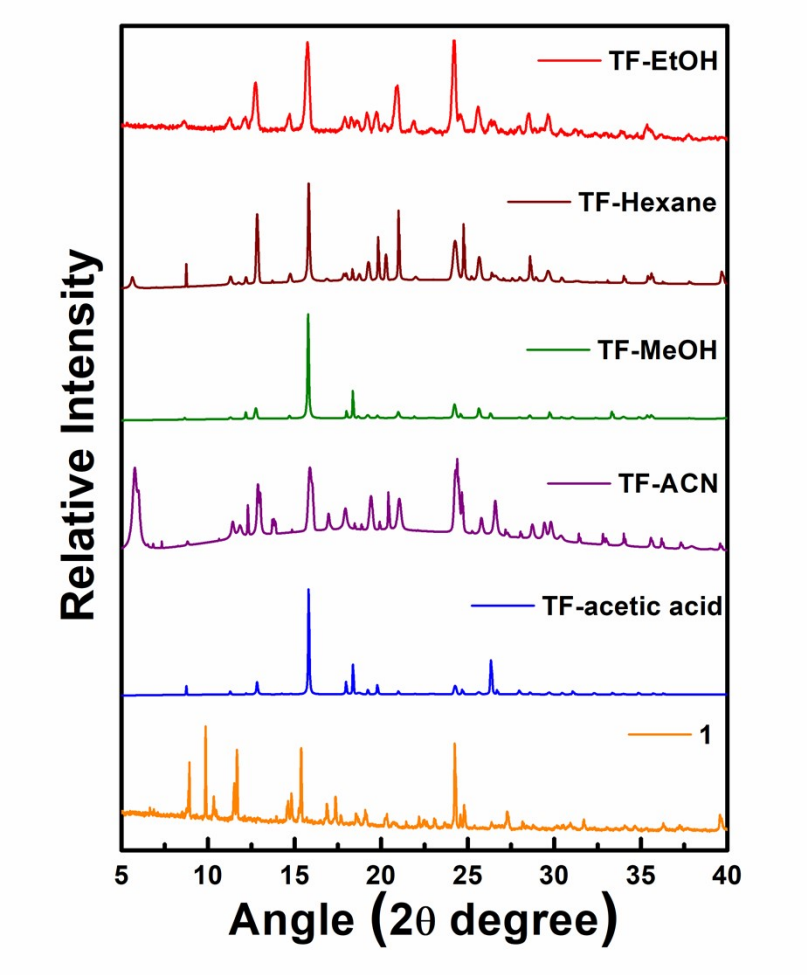

Figure S-21: PXRD of thin films in ETOH, MeOH, ACN, acetic acid and Hexane of **1.**

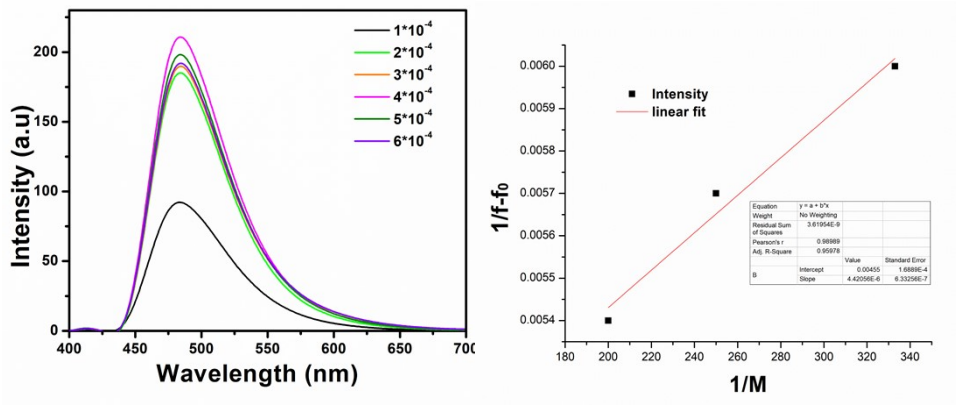

Figure S-22: Fluorescence spectra obtained by titration of different concentrations of methanolic solution of zn (II) ions against 10^{-4}M methanolic solution of **2** and its linear fit for calculation of binding constant.

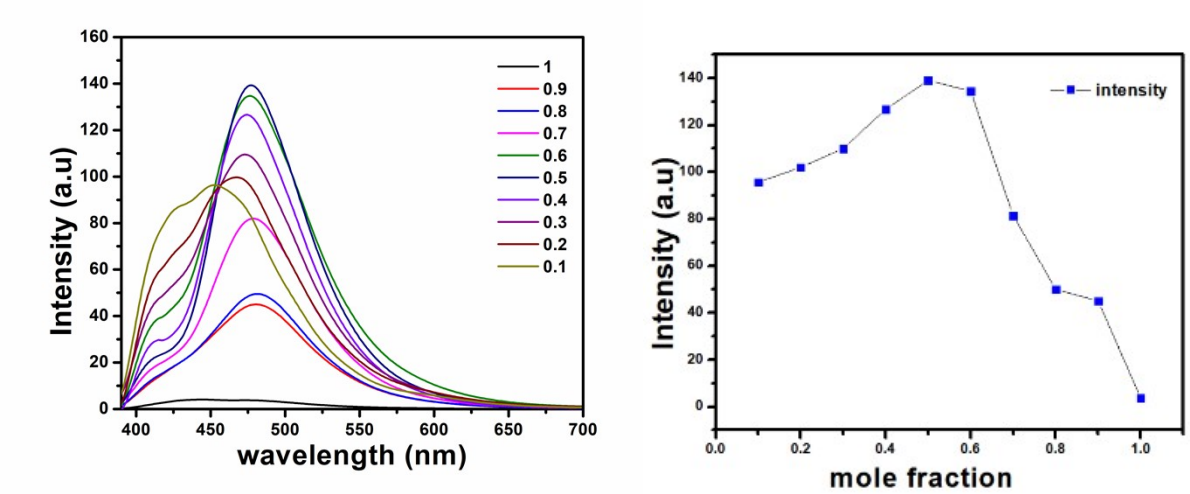

Figure S-23: Job (continuous variation) plot by mixing equimolar total concentrations of compound 2 and Zn(II) while varying the mole fraction of Zn(II) and 2 and keeping the total concentration constant, for determing the stichometry of metal ligand complex.

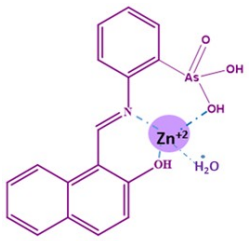

Figure S-24: Tetrahedral metal complex of schiff base **2** with zn(II).

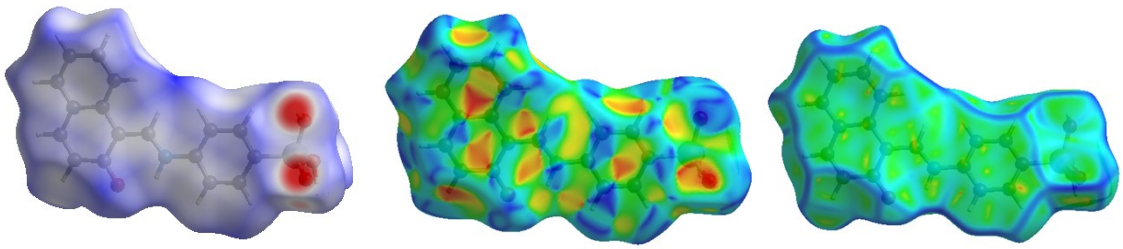

Figure S-25: d_{norm}, Shape-index, and Curvedness surface of molecular solid **1**.

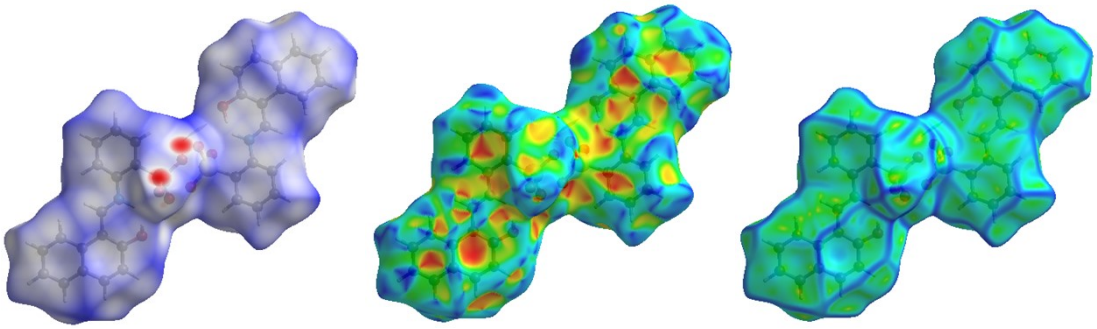

Figure S-26: d_{norm}, Shape-index, and Curvedness surface of molecular solid **2.**

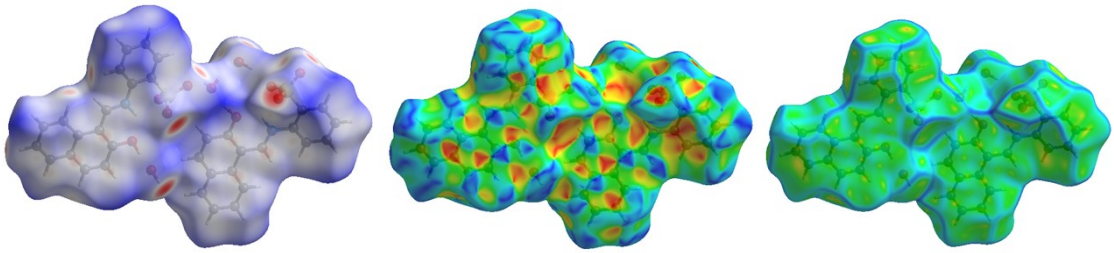

Figure S-27: d_{norm}, Shape-index, and Curvedness surface of molecular solid **3**.

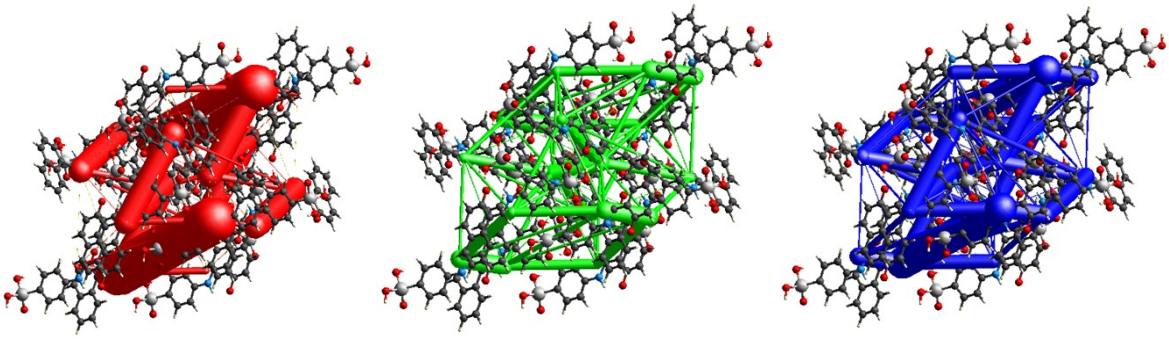

Figure S-28: Columb energy, dispersion energy, and total energy calculations of **1.**

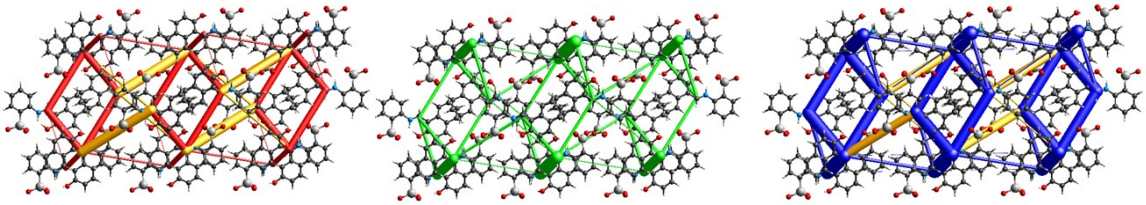

Figure S-29: Columb energy, dispersion energy, and total energy calculations of **2.**

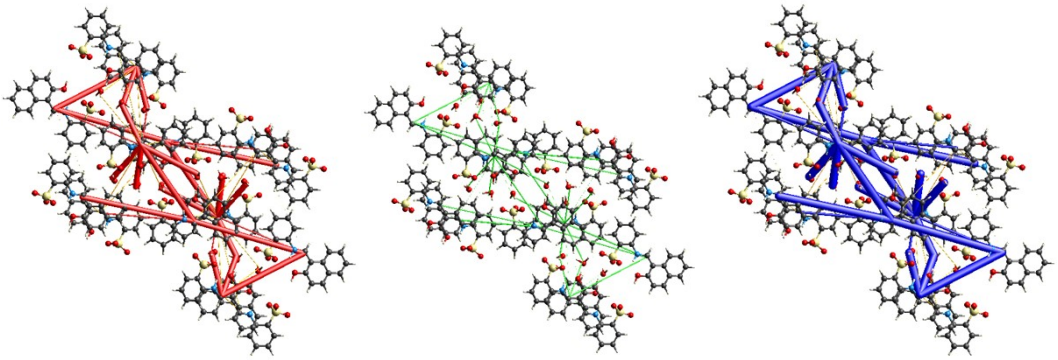

Figure S-30: Columb energy, dispersion energy, and total energy calculations of **3.**

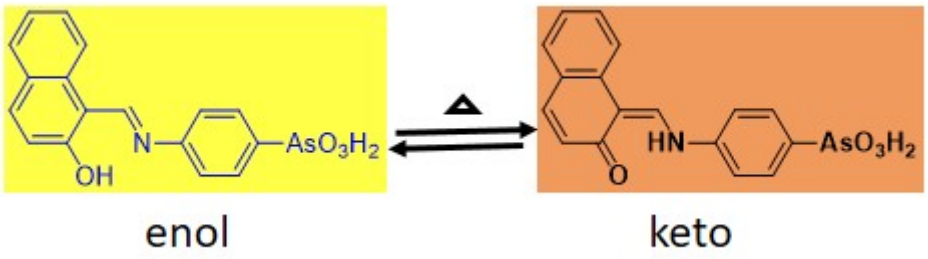

Figure S-31: Mechanism of Keto-Enol tautomerism.

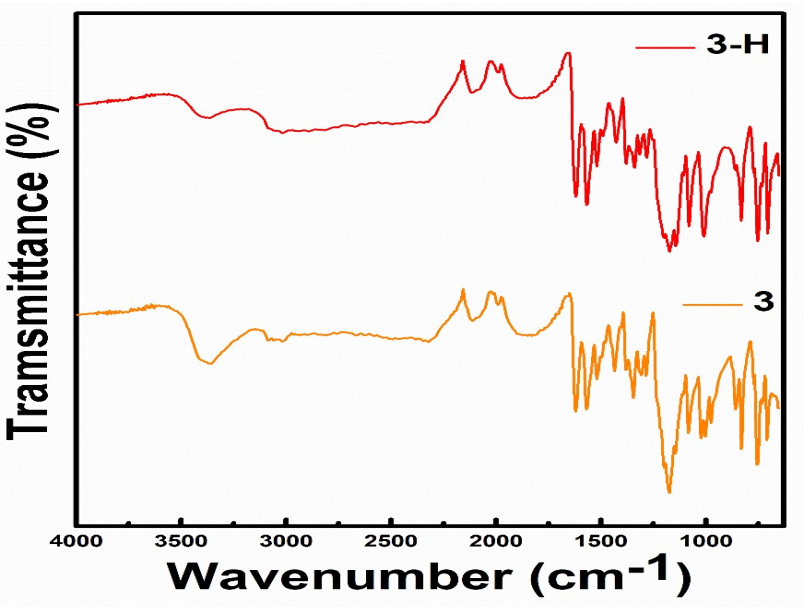

Figure S-32: FTIR of **3** and **3H**.

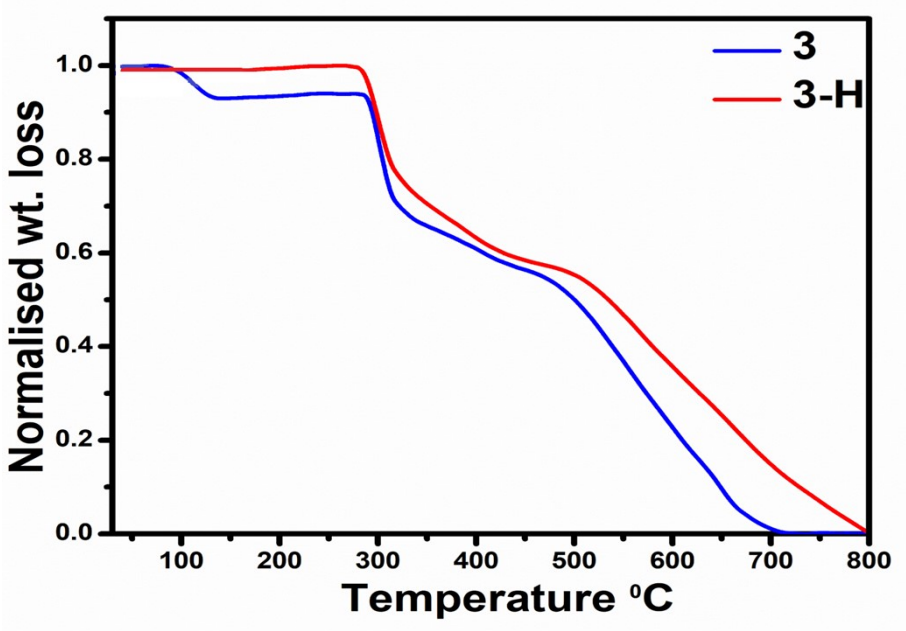

Figure S-33: TGA of **3** and **3H**.

Figure S-34: Thermochromic photoghaphs under different conditions in **3H**.

Table S-1: Crystallographic Table of **1-3**

Reaction code/Compounds	**AI-322(1)**	**AI-318(2)**	**SF-12 (3)**
CCDC No.	2444241	2444242	2444243
Empirical formula	C17 H14 As N O4	C17 H14 As N O4	2(C17 H13 N O4 S), H3 O,2(H2 O)
Fw	371.21	371.21	708.73
Temp [K]	150	149	150
Crystal system	Monoclinic	Monoclinic	Monoclinic
Space group	P 21/n	P 21/c	P 21/c
a, [Å]	11.5840(11)	15.570(13)	6.6530(8)
b, [Å]	9.4113(9)	7.045(5)	17.223(2)
c, [Å]	14.1627(13)	27.48(2)	27.491(4)
α, [°]	90	90	90
β, [°]	105.590(3)	99.94(2)	93.369(3)

γ, [°]	90	90	90
V, [Å^3]	1487.2(2)	2969(4)	3144.6(7)
Z	4	8	4
D(calcd) [Mg/cm^3]	1.658	1.661	1.497
μ [mm^{-1}]	2.306	2.310	0.238
Θ range [°]	28.346	24.988	28.458
Reflns collected	3719	5167	7880
Indep. Reflns	3242	3524	3387
GOF	0.986	1.140	0.948
R1(I_0>2σ(I_0)	0.0258	0.1026	0.0678
wR2(all data)	0.0584	0.2796	0.1894

Table S-2: The calculated energy levels for **1-3**

	E(HOMO)/eV	E(LUMO)/eV	ΔE/eV	E_g/eV
1	-5.27	-3.55	1.72	2.21
2	-5.22	-3.29	1.93	2.27
3	-4.94	-3.19	1.75	2.23

ΔE is the bandgap obtained from cyclic voltammetry. E_g is the optical band gap calculated UV-vis absorption spectroscopy.

Table S-3: LODs values of some selective zinc sensors.

S.NO	Sensor Type	LOD	reference
1	(2-((3-morpholinopropyl)amino)-N-(quinolin-8-yl)acetamide)	0.29 x 10^{-6}M	1
2	Benzothiazole-based (BIPP)	2.36 x 10^{-8} M	2
3	Salen-based probe	2.18 x 10^{-6} M	3
4	shiff base (2)	4.9x 10^{-6} M	This work
5	2-(quinolin-2-yl)quinazolin-4(3H)-one	8.82×10^{-7}M.	4
6	Pyrene-malonohydrazide derivative	5.1× 10^{-9} M	5
7	zinc sensor based on quinoline	0.63x 10^{-6} M	6

Table S-4: Interaction and lattice energy calculation of **1.**

	N	Symop	R	Electron Density	E_ele	E_pol	E_dis	E_rep	E_tot
	1	-x, -y, -z	10.89	HF/3-21G	-205.2	-78.4	-24.8	177.7	-138.4
	2	-x+1/2, y+1/2, -z+1/2	7.73	HF/3-21G	-109.5	-36.4	-23.6	95.9	-78.7
	1	-x, -y, -z	5.89	HF/3-21G	-25.1	-5.9	-86.0	35.0	-78.6
	0	-x, -y, -z	5.87	HF/3-21G	-31.9	-12.1	-47.3	24.6	-63.1
	1	x+1/2, -y+1/2, z+1/2	11.21	HF/3-21G	0.6	-2.1	-3.9	0.2	-4.1
	2	x+1/2, -y+1/2, z+1/2	9.04	HF/3-21G	1.4	-1.6	-5.3	0.6	-3.9
	2	x+1/2, -y+1/2, z+1/2	9.28	HF/3-21G	-2.1	-1.6	-11.9	5.2	-9.7
	1	x+1/2, -y+1/2, z+1/2	11.41	HF/3-21G	-1.4	-1.1	-16.1	7.7	-10.4
	0	-x, -y, -z	11.30	HF/3-21G	1.4	-3.0	-52.6	25.0	-27.6
	2	-x+1/2, y+1/2, -z+1/2	9.31	HF/3-21G	1.0	-2.1	-14.9	7.0	-8.0
	2	-x+1/2, y+1/2, -z+1/2	12.25	HF/3-21G	-1.0	-0.5	-2.5	0.0	-3.6
	1	x, y, z	14.93	HF/3-21G	-13.6	-2.4	-15.0	0.0	-28.9

Table S-5: Interaction and lattice energy calculation of **2.**

	N	Symop	R	Electron Density	E_ele	E_pol	E_dis	E_rep	E_tot
	0	-	13.76	HF/3-21G	0.0	-10.7	0.0	0.0	-7.0
	0	-	8.11	HF/3-21G	-4.6	-19.9	-25.4	16.6	-27.0
	0	-x, -y, -z	6.36	HF/3-21G	-35.8	-20.2	-96.5	48.6	-97.2
	0	x, -y+1/2, z+1/2	13.74	HF/3-21G	0.0	-2.5	0.0	0.0	-1.6
	0	-x, -y, -z	6.52	HF/3-21G	-34.6	-25.0	-75.4	36.2	-90.1
	0	-x, y+1/2, -z+1/2	11.04	HF/3-21G	-13.7	-1.5	-8.6	1.5	-21.3
	0	-	8.43	HF/3-21G	-37.1	-11.7	-23.2	7.0	-60.6
	1	-	9.01	HF/3-21G	65.2	-29.5	-17.2	29.1	55.3
	0	-	9.13	HF/3-21G	-45.6	-20.3	-22.5	12.5	-69.9
	0	-	11.54	HF/3-21G	18.1	-3.0	-9.5	4.1	11.2
	0	-	8.16	HF/3-21G	-47.4	-21.2	-27.7	11.4	-77.8
	0	-	9.36	HF/3-21G	52.1	-21.4	-17.8	27.0	45.0

Table S-6: Interaction and lattice energy calculation of **3.**

	N	Symop	R	Electron Density	E_ele	E_pol	E_dis	E_rep	E_tot
	2	x, y, z	14.23	HF/3-21G	-19.1	-11.9	-11.1	0.0	-37.2
	2	x+1/2, -y+1/2, -z	9.64	HF/3-21G	-21.2	-8.2	-9.4	1.0	-34.6
	2	-x+1/2, y+1/2, z	8.69	HF/3-21G	-19.8	-20.1	-64.0	31.7	-65.2
	1	-x, -y, -z	12.48	HF/3-21G	-6.4	-2.8	-15.3	0.0	-22.2
	2	-x, y+1/2, -z+1/2	9.49	HF/3-21G	-43.9	-37.1	-38.5	18.7	-88.3
	2	-x+1/2, y+1/2, z	11.04	HF/3-21G	-10.1	-28.1	-12.3	7.4	-33.7
	1	-x, -y, -z	6.85	HF/3-21G	-167.6	-87.0	-96.7	86.5	-244.4
	2	x+1/2, -y+1/2, -z	13.65	HF/3-21G	-90.5	-45.2	-13.4	0.0	-133.7
	2	x+1/2, y, -z+1/2	9.03	HF/3-21G	32.8	-7.2	-39.5	20.1	9.5

1. D. Yun, J. B. Chae, H. So, H. Lee, K.-T. Kim and C. Kim, Sensing of zinc ions and sulfide using a highly practical and water-soluble fluorescent sensor: applications in test kits and zebrafish, *New J. Chem.*, 2020, **44**, 442-449.
2. S. Enbanathan, S. Munusamy, D. Jothi, S. Manojkumar, S. Manickam and S. K. Iyer, Zinc ion detection using a benzothiazole-based highly selective fluorescence “turn-on” chemosensor and its real-time application, *RSC Adv.*, 2022, **12**, 27839-27845.
3. B. Das, M. Dolai, A. Dhara, S. Mabhai, A. Jana, S. Dey and A. Misra, Acetate ion augmented fluorescence sensing of Zn2+ by Salen-based probe, AIE character, and application for picric acid detection, *Anal. Sce. Adv.*, 2021, **2**, 447-463.
4. X.-J. Bai, J. Ren, J. Zhou and Z.-B. Song, A ‘turn-on’fluorescent chemosensor for the detection of Zn2+ ion based on 2-(quinolin-2-yl) quinazolin-4 (3 H)-one, *Heterocyclic Commun.*, 2018, **24**, 135-139.
5. B. K. Rani and S. A. John, A highly selective turn-on fluorescent chemosensor for detecting zinc ions in living cells using symmetrical pyrene system, *J. Photochem. and Photobiol. A.*, 2021, **418**, 113372.
6. J. M. Jung, J. J. Lee, E. Nam, M. H. Lim, C. Kim and R. G. Harrison, A zinc fluorescent sensor used to detect mercury (II) and hydrosulfide, *SAA*, 2017, **178**, 203-211.